J|A|C|S COMMUNICATIONS

Published on Web 10/11/2010

Nanocrystal Superlattices with Thermally Degradable Hybrid Inorganic−Organic Capping Ligands

Maksym V. Kovalenko,* Maryna I. Bodnarchuk, and Dmitri V. Talapin*

Department of Chemistry and James Frank Institute, University of Chicago, Chicago, Illinois 60637, United States

Received July 30, 2010; E-mail: mvkovalenko@uchicago.edu; dvtalapin@uchicago.edu

Abstract: Colloidal metallic and semiconductor nanocrystals (NCs) functionalized with metal chalcogenide complexes (MCCs) have shown a promise for designing materials that combine high carrier mobility with the electronic structure of strongly quantum-confined solids. Here we report a simple and general methodology for switching the repulsive forces responsible for colloidal stabilization of MCC-capped NCs from long-range electrostatic to short-range steric through the formation of tight ionic pairs with cationic surfactants. This noncovalent surface modification remarkably improved the ability of MCC-capped NCs to self-assemble into long-range ordered superlattices. These NCs are highly soluble in nonpolar solvents and compatible with various technologically relevant organic molecules and polymers. The hybrid inorganic−organic coating can be thermally decomposed at significantly lower temperatures compared to those required for removal of conventional organic ligands.

New methods for programmable design of solid-state materials from chemically synthesized nanocrystals (NCs) are becoming increasingly important because of their high potential for electronic and optoelectronic applications.[1] The surface chemistry determines compatibility of colloidal NCs with other moieties and their ability to form long-range ordered and electronically coupled NC assemblies. We have recently developed a new type of surface coatings by using metal chalcogenide complexes (MCCs, also known as chalcogenidometalates) such as $Sn_2S_6^{4-}$, $SnTe_4^{4-}$, AsS_3^{3-}, etc.,[2,3] which enabled the fabrication of dense nanostructured solids with advanced electronic and thermoelectric characteristics.[2,4,5]

Surface charges stabilize colloidal solutions of MCC-capped NCs in polar solvents such as water, hydrazine, and formamide (FA). At the same time, long-range electrostatic repulsion between the NCs negatively affects their ability to self-assemble into ordered superlattices. With the aim to (i) reduce the Coulomb repulsion and (ii) expand the compatibility of MCC-capped NCs with common nonpolar solvents and molecules, we developed a simple method for turning the surface of MCC-capped NCs from highly hydrophilic to nonpolar and lipophilic. Our approach is based on the ability of cationic surfactant molecules to bind to negatively charged surfaces, forming dense, hydrophobic monolayers.[6−8] As the model systems we used FA solutions of metallic (Au, Pd), magnetic (FePt), and semiconducting (PbS, PbSe, CdSe, CdS) NCs stabilized with Na_3AsS_3 or $(NH_4)_3AsS_3$ surface ligands.[3,9]

To form a hydrophobic coating, Na^+ or NH_4^+ counterions were partially replaced with different tertiary alkylammonium ions (Figure 1A). As an example, didodecyldimethylammonium bromide (DDAB) was used as a source of DDA^+ hydrophobic cations.[9] In a typical cation-exchange procedure,[9] a FA solution of MCC-capped NCs was mixed with a toluene solution of DDAB, first leading to the aggregation of NCs followed by their fast phase transfer into the toluene phase, forming a stable colloidal solution. We also observed complete phase transfer using other combinations of MCCs, NCs, and solvents, such as solutions of $Sn_2Se_6^{4-}$, $In_2Se_4^{2-}$, and $SnTe_4^{4-}$-capped CdSe NCs in hydrazine. Other long-chain cationic surfactants, such as cetylpyridinium bromide, can be used instead of tertiary alkylammonium salts.

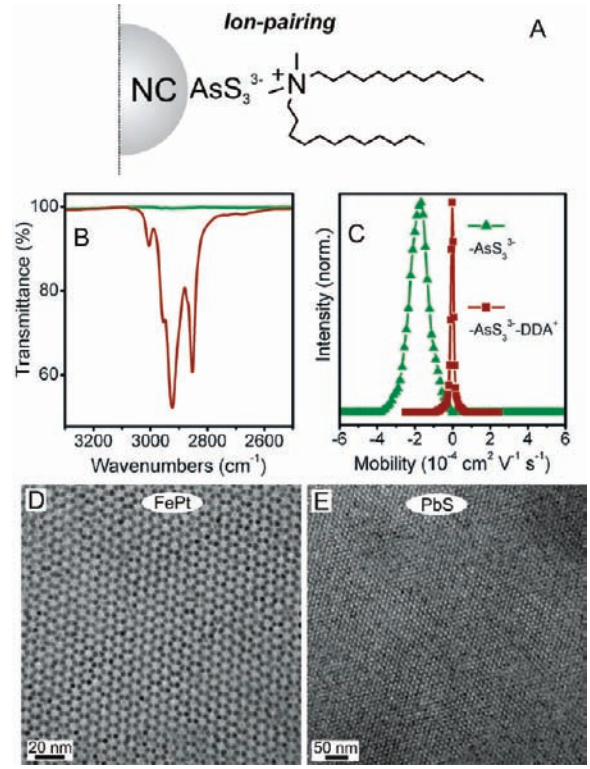

Figure 1. (A) Schematics of a NC with hybrid inorganic (AsS_3^{3-})−organic (DDA^+) surface coating. (B) FTIR spectra for Na_3AsS_3-stabilized PbS NCs (green) and DDA^+-AsS_3^{3-}-capped PbS NCs (red) with 3.7 nm PbS core size. (C) Electrophoretic mobility measurements for Na_3AsS_3-stabilized PbS NCs in FA (green) and DDA^+-AsS_3^{3-}-capped PbS NCs in toluene (red) with 10 nm PbS core diameter. (D,E) TEM images showing hexagonal close-packed lattices of DDA^+-AsS_3^{3-}-capped 3.8 nm FePt NCs (D) and 7.2 nm PbS NCs (E).

The FTIR spectra of purified DDA^+-AsS_3^{3-}-PbS NCs (Figure 1B) exhibited characteristic C−H stretching vibrations, not present in the original Na_3AsS_3-stabilized NCs. Elemental analysis by inductively coupled plasma optical emission spectroscopy (ICP-OES) showed that the As content remained unchanged during the cation exchange (PbS:As $\approx$ 3.4:1 for $\sim$3.5 nm PbS cores), while at least 60% Na^+ was displaced by DDA^+. The complete exchange of Na^+ with DDA^+ might be prohibited by steric crowding of several bulky DDA^+ ions in close proximity to AsS_3^{3-} groups.

The efficient ion-pairing between MCC anions and DDA^+ is evident from the electrophoretic mobility (μ) measurements (Figure

10.1021/ja106841f

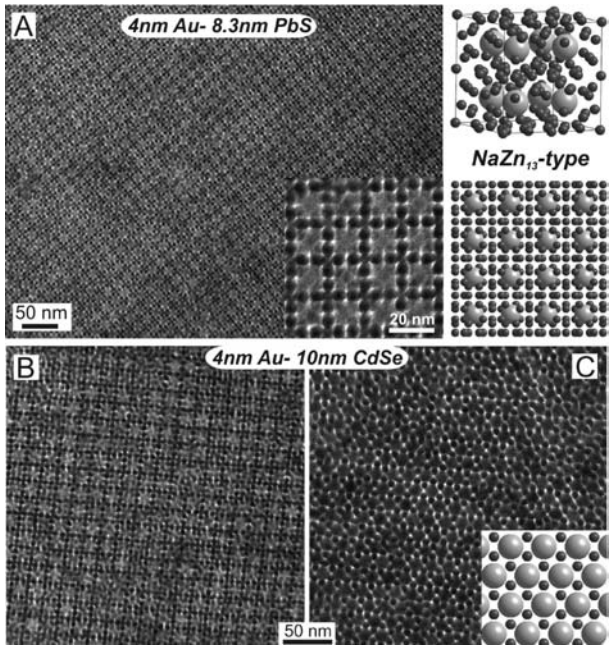

Figure 2. TEM images of binary NC superlattices self-assembled from DDA^+-AsS_3^{3-}-capped NCs. (A) $NaZn_{13}$-type BNSL composed of 4 nm Au NCs and 8.3 nm PbS NCs. Panels on the right illustrate the unit cell consisting of 104 arranged small spheres and 8 large spheres (top) and (100) projection of $NaZn_{13}$ lattice (bottom).[10] (B,C) $NaZn_{13}$ and AlB_2-type BNSLs self-assembled from 4 nm Au NCs and 10 nm CdSe NCs. Inset in (C) shows (001) projection of AlB_2 lattice.

1C).[9] Pristine Na_3AsS_3-stabilized PbS NCs showed $\mu \approx 1.8 \times 10^{-8}$ $m^2\ V^{-1}\ s^{-1}$ in FA, corresponding to the surface charge density (σ) of 0.051 C/m^2 or ~125 elemental charges (e) per NC (~10 nm PbS core size).[9] Ion-pairing with DDA^+ resulted in a decrease of μ to 0.0218×10^{-8} $m^2\ V^{-1}\ s^{-1}$, corresponding to less than 0.1e per NC.[11] Tight ion-pairing provided charge neutrality up to at least 80 °C. Dynamic light scattering (DLS) measurements taken at each step of surface functionalization (Figure S2, Supporting Information) indicated very similar hydrodynamic radii within ±0.5 nm and single-particle populations, confirming the absence of any mesoscopic or macroscopic aggregates of NCs.

The long hydrocarbon chains stabilize colloidal solutions via steric repulsion.[12] The absence of long-range electrostatic repulsion caused a strong tendency of DDA^+-MCC^{n-}-capped NCs to form long-range ordered superlattices through standard drying-mediated self-assembly[11,13−16] from their toluene/tetrachloroethylene solutions (Figures 1D,E, 2, and S3−S7 (Supporting Information)). In contrast, the original highly charged MCC-capped NCs formed disordered structures,[2−4] with the only exception for Au NC superlattices.[2] The recent studies on self-assembly of NCs capped with conventional long-chain organic ligands have pointed to a complex balance of forces determining the changes in the free energy, $F = U - TS$, associated with the self-assembly process.[17,18] Self-assembly of colloidal NCs is typically driven by changes in the free-volume entropy, often combined with weak attractive interparticle forces.[17,19] The ideal case for the entropy-driven self-assembly is when the NCs exhibit only short-range repulsion associated with direct ligand−ligand interactions.[20,21]

In the case of binary superlattices, the gain in free volume entropy is related to the packing density (e.g., space-filling fraction ρ) at a given effective size ratio of small to large NCs ($\gamma_{eff} = d_{small}/d_{large}$, see Figure S8, Supporting Information). Generally, it favors the structures with highest ρ.[11,21,22] We studied the combinations of smaller metallic (Au, Pd, FePt) with larger semiconductor (CdSe, PbS, PbSe) NCs, corresponding to the γ_{eff} range of 0.56−0.64. A shell thickness of ~1.8 nm was estimated for DDA^+-AsS_3^{3-} capping[9] and was added to NC core diameters to calculate γ_{eff}.

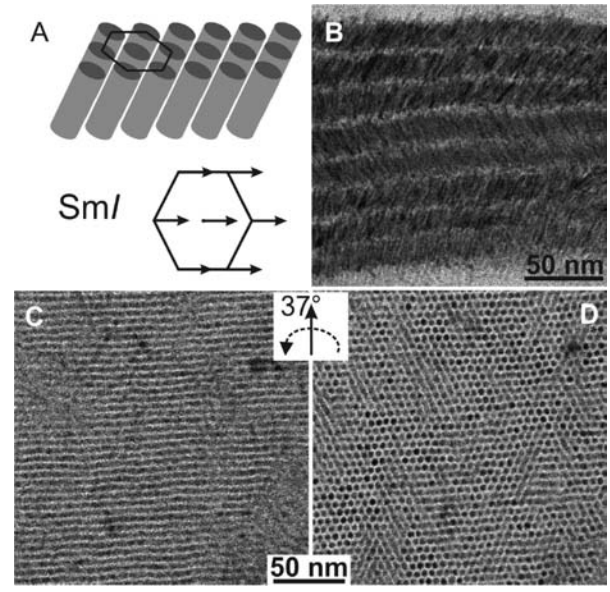

Figure 3. (A) Illustration of the smectic-I (SmI) phase formed by tilting an array of hexagonally ordered rods toward the apex of the hexagon. (B) TEM images of the "tracks" of 4 × 28 nm CdS nanorods (NRs) with aspect ratio $L/D \approx 4$ (including ligand shell thickness). (C,D) A monolayer of self-assembled CdS NRs viewed (C) normal to the substrate and (D) tilted by 37°.

The NCs with hybrid DDA^+-AsS_3^{3-} coating self-assembled into two binary nanocrystal superlattice (BNSL) phases isostructural with $NaZn_{13}$ and AlB_2 (Figure 2). These lattices have the highest ρ among known binary structures for the selected γ_{eff} range (Figure S8). Both $NaZn_{13}$ and AlB_2 were predicted to be thermodynamically stable phases in the mixtures of hard spheres.[20,23,24] The coexistence of $NaZn_{13}$ and AlB_2 phases has been observed in BNSLs at similar γ_{eff} values,[10] as well as in mixtures of micrometer-sized particles.[22,25] In our case, $NaZn_{13}$ BNSLs readily formed for all studied NC combinations, while the AlB_2 phase formed with appreciable yield only at $\gamma_{eff} \approx 0.56$ and was not observed at $\gamma_{eff} \approx 0.64$, where $NaZn_{13}$ has much lower density ($\rho \approx 0.66$). The dominant formation of $NaZn_{13}$-type structure can be explained by the higher contribution from the internal energy U due to efficient van der Waals interactions within the icosahedral clusters of metal NCs.[17] Another plausible explanation could arise from the kinetic factors,[22] which may include a lower nucleation barrier for $NaZn_{13}$[20] or preassembly of smaller metal particles into icosahedral clusters in solution before their integration into BNSL.[26]

Monodisperse colloidal nanorods (NRs) represent an ideal system for studying self-organization of anisotropic objects, driven by both the entropy[27] and specific forces such as dipole−dipole interactions between NRs and between NRs and substrate.[28,29]

We found that monodisperse CdS NRs, capped with the original alkyl phosphonate ligands, formed the hexatic smectic-B (hex$B$) liquid-crystalline phase[30] (Figure S9, Supporting Information), in agreement with the previous studies of Cd−chalcogenide NRs self-assembly.[29,31,32] In contrast, self-assembly of DDA^+-AsS_3^{3-}-capped CdS NRs yielded the smectic-I (SmI) phase (Figure 3),[30] previously unknown for inorganic NRs. SmI can be viewed as the tilted analogue of the hex$B$ phase. The tilt angle of 30−40° can be seen in the "tracks" of lying NRs (Figure 3B) and in the TEM in situ tilting studies of the domains of standing NRs. When viewed normal to the substrate, the assemblies

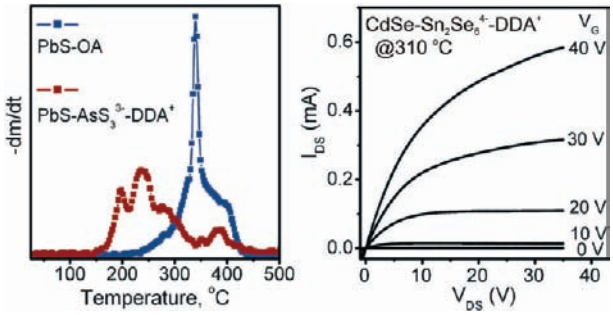

Figure 4. (A) Differential thermogravimetric data for 3.7 nm diameter PbS NCs capped with oleic acid (blue) and with DDA^+-AsS_3^{3-} hybrid coating (red). (B) Plot of source-drain current vs source-drain voltage for an FET with the channel composed of 5 nm CdSe NCs capped with DDA^+-$Sn_2Se_6^{4-}$ and annealed at 310 °C (channel length 20 μm, width 1800 μm, 110-nm-thick SiO_2 gate dielectric). CdSe-$Sn_2Se_6^{4-}$ NCs were prepared in N_2H_4,[2] functionalized with DDA^+, and dispersed in toluene as described in the Supporting Information.

of DDA^+-AsS_3^{3-}-capped CdS NRs appear as parallel stripes (Figure 3C). Tilting the TEM grid to 37° revealed long-range hexagonal ordering of CdS nanorods (Figure 3D).[33]

The formation of Sm*I* phase from DDA^+-AsS_3^{3-}-capped CdS NRs could be explained by their structural analogies with the previously studied rod−coil diblock copolymers, which also formed tilted phases (smectic-*C*, with no positional ordering within the lamella).[34] It was shown that rigid rods grafted with soft molecular chains (coils) form tilted liquid-crystalline phases to maximize the exposure of coils to the solvent. Such exposure reduces both surface energy and the steric constraint generated at the side surfaces of the rods.[34]

Thermogravimetric analysis (TGA) for DDA^+-AsS_3^{3-}-PbS NCs revealed several decomposition events starting at ∼160 °C (Figures 4A and S10 (Supporting Information)). This behavior is in striking contrast to that of PbS NCs with conventional organic ligands such as oleic acid, which decompose well above 300 °C. Thermal degradation of tetraalkylammonium ions occurs typically through Hofmann elimination.[35] It is also known that thermal decomposition of metal sulfide (selenide) compounds, charge-balanced with the alkylammonium ions, generates metal chalcogenides and a mixture of alkanes, alkenes, alkyl sulfides (selenides), and disulfides.[36−38]

The reduced thermal onset for removal of hybrid surface ligands allows fabricating semiconducting films that can be used in field-effect transistors (FETs, Figure 4B). The FETs made of CdSe NCs capped with DDA^+-$Sn_2Se_6^{4-}$ ligands showed linear and saturation regime electron mobilities of ∼0.6 and 0.9 $cm^2\ V^{-1}\ s^{-1}$, respectively (Figure S11, Supporting Information), and an on/off current ratio of $\sim 10^3-10^4$. In contrast, no operational FETs could be fabricated from CdSe NCs capped with conventional organic ligands because the NC films remained highly insulating up to at least 380 °C annealing temperatures.

In summary, we demonstrated a simple noncovalent encapsulation of MCC-capped NCs using cationic surfactants. This approached allowed the facile formation of ordered superlattices of MCC-capped NCs and the compatibility of MCC-capped NCs with common nonpolar molecules. As compared to conventional covalently attached organic ligands, the cationic surfactant monolayers can be removed at much lower temperatures, leading to electronically conductive and long-range-ordered NC solids.

Acknowledgment. The work was supported by NSF CAREER under Award No. DMR-0847535 and by the Office of Naval Research under Award No. N00014-10-1-0190. D.V.T. thanks the David and Lucile Packard Foundation for their generous support. The Analytical Chemistry Laboratory at Argonne National Laboratory (ANL) carried out the elemental analysis of NC samples. The work at the Center for Nanoscale Materials (ANL) was supported by the U.S. Department of Energy under Contract No. DE-AC02-06CH11357.

Supporting Information Available: Materials and Methods, TEM, DLS, and space-filling curves. This material is available free of charge via the Internet at http://pubs.acs.org.

References

(1) Talapin, D. V.; Lee, J. S.; Kovalenko, M. V.; Shevchenko, E. V. *Chem. Rev.* **2010**, *110*, 389–458.
(2) Kovalenko, M. V.; Scheele, M.; Talapin, D. V. *Science* **2009**, *324*, 1417–1420.
(3) Kovalenko, M. V.; Bodnarchuk, M. I.; Zaumseil, J.; Lee, J.-S.; Talapin, D. V. *J. Am. Chem. Soc.* **2010**, *132*, 10085–10092.
(4) Kovalenko, M. V.; Spokoyny, B.; Lee, J. S.; Scheele, M.; Weber, A.; Perera, S.; Landry, D.; Talapin, D. V. *J. Am. Chem. Soc.* **2010**, *132*, 6686–6695.
(5) Tangirala, R.; Baker, J. L.; Alivisatos, A. P.; Milliron, D. J. *Angew. Chem., Int. Ed.* **2010**, *49*, 2878–2882.
(6) Heinz, H.; Suter, U. W. *Angew. Chem., Int. Ed.* **2004**, *43*, 2239–2243.
(7) Volkmer, D.; Du Chesne, A.; Kurth, D. G.; Schnablegger, H.; Lehmann, P.; Koop, M. J.; Muller, A. *J. Am. Chem. Soc.* **2000**, *122*, 1995–1998.
(8) Kurth, D. G.; Lehmann, P.; Lesser, C. *Chem. Commun.* **2000**, 949–950.
(9) See Supporting Information for more details.
(10) Chen, J.; Ye, X. C.; Murray, C. B. *ACS Nano* **2010**, *4*, 2374–2381.
(11) Balandin, A. A.; Lazarenkova, O. L. *Appl. Phys. Lett.* **2003**, *82*, 415–417.
(12) *Nanoparticles—From Theory to Applications*; Schmid, G., Ed.; Wiley-VCH: Weinheim, 2004.
(13) Redl, F. X.; Cho, K. S.; Murray, C. B.; O'Brien, S. *Nature* **2003**, *423*, 968–971.
(14) Shevchenko, E. V.; Talapin, D. V.; Kotov, N. A.; O'Brien, S.; Murray, C. B. *Nature* **2006**, *439*, 55–59.
(15) Evers, W. H.; Friedrich, H.; Filion, L.; Dijkstra, M.; Vanmaekelbergh, D. *Angew. Chem., Int. Ed.* **2009**, *48*, 9655–9657.
(16) Smith, D. K.; Goodfellow, B.; Smilgies, D. M.; Korgel, B. A. *J. Am. Chem. Soc.* **2009**, *131*, 3281–3290.
(17) Bodnarchuk, M. I.; Kovalenko, M. V.; Heiss, W.; Talapin, D. V. *J. Am. Chem. Soc.* **2010**, *132*, 11967–11977.
(18) Talapin, D. V. *ACS Nano* **2008**, *2*, 1097–1100.
(19) Chen, Z.; O'Brien, S. *ACS Nano* **2008**, *2*, 1219–1229.
(20) Eldridge, M. D.; Madden, P. A.; Frenkel, D. *Nature* **1993**, *365*, 35–37.
(21) Murray, M. J.; Sanders, J. V. *Philos. Mag. A* **1980**, *42*, 721–740.
(22) Hunt, N.; Jardine, R.; Bartlett, P. *Phys. Rev. E* **2000**, *62*, 900–913.
(23) Eldridge, M. D.; Madden, P. A.; Frenkel, D. *Mol. Phys.* **1993**, *80*, 987–995.
(24) Eldridge, M. D.; Madden, P. A.; Frenkel, D. *Mol. Phys.* **1993**, *79*, 105–120.
(25) Sanders, J. V. *Philos. Mag. A* **1980**, *42*, 705–720.
(26) Keys, A. S.; Glotzer, S. C. *Phys. Rev. Lett.* **2007**, *99*, 235503.
(27) Frenkel, D.; Lekkerkerker, H. N. W.; Stroobants, A. *Nature* **1988**, *332*, 822–823.
(28) Titov, A. V.; Kral, P. *Nano Lett.* **2008**, *8*, 3605–3612.
(29) Talapin, D. V.; Shevchenko, E. V.; Murray, C. B.; Kornowski, A.; Forster, S.; Weller, H. *J. Am. Chem. Soc.* **2004**, *126*, 12984–12988.
(30) *Liquid Crystals*; Stegemeyer, H., Ed.; Springer: New York, 1994.
(31) Carbone, L.; et al. *Nano Lett.* **2007**, *7*, 2942–2950.
(32) Baker, J. L.; Widmer-Cooper, A.; Toney, M. F.; Geissler, P. L.; Alivisatos, A. P. *Nano Lett.* **2010**, *10*, 195–201.
(33) Alternative tilting toward the side of the hexagon is also known in molecular liquid crystals and is classified as smectic-*F* phase.
(34) Halperin, A. *Macromolecules* **1990**, *23*, 2724–2731.
(35) Xie, W.; Gao, Z. M.; Pan, W. P.; Hunter, D.; Singh, A.; Vaia, R. *Chem. Mater.* **2001**, *13*, 2979–2990.
(36) Li, J. Q.; Marler, B.; Kessler, H.; Soulard, M.; Kallus, S. *Inorg. Chem.* **1997**, *36*, 4697–4701.
(37) Jiang, T.; Ozin, G. A.; Bedard, R. L. *Adv. Mater.* **1995**, *7*, 166–170.
(38) Trikalitis, P. N.; Ding, N.; Malliakas, C.; Billinge, S. J. L.; Kanatzidis, M. G. *J. Am. Chem. Soc.* **2004**, *126*, 15326–15327.

JA106841F